Generation of the R2 Subunit of Ribonucleotide Reductase by Intein Chemistry: Insertion of 3-Nitrotyrosine at Residue 356 as a Probe of the Radical Initiation Process†

Cyril S. Yee,‡ Mohammad R. Seyedsayamdost,‡ Michelle C. Y. Chang,‡ Daniel G. Nocera,‡ and JoAnne Stubbe*,‡,§

Departments of Chemistry and Biology, Massachusetts Institute of Technology, Cambridge, Massachusetts 02139

Received July 14, 2003; Revised Manuscript Received October 22, 2003

ABSTRACT: *Escherichia coli* ribonucleotide reductase (RNR) catalyzes the conversion of nucleoside diphosphates to deoxynucleoside diphosphates. The enzyme is composed of two subunits: R1 and R2. R1 contains the active site for nucleotide reduction and the allosteric effector sites that regulate the specificity and turnover rate. R2 contains the diferric-tyrosyl (Y•) radical cofactor that initiates nucleotide reduction by a putative long-range proton-coupled electron transfer (PCET) pathway over 35 Å. This pathway is thought to involve specific amino acid radical intermediates (Y122 to W48 to Y356 within R2 to Y731 to Y730 to C439 within R1). In an effort to study radical initiation, R2 (375 residues) has been synthesized semisynthetically. R2 (residues 1−353), attached to an intein and a chitin binding domain, was constructed, and the protein was expressed (construct 1). This construct was then incubated with Fe^{2+} and O_2 to generate the diferric-Y• cofactor, and the resulting protein was purified using a chitin affinity column. Incubation of construct 1 with 2-mercaptoethanesulfonic acid (MESNA) resulted in the MESNA thioester of R2 (1−353) (construct 2). A peptide containing residues 354−375 of R2 was generated using solid-phase peptide synthesis where 354, a serine in the wild-type (wt) R2, was replaced by a cysteine. Construct 2 and this peptide were ligated, and the resulting full-length R2 was separated from truncated R2 by anion-exchange chromatography. The purified protein had a specific activity of 350 nmol min^{-1} mg^{-1}, identical to the same protein generated by site-directed mutagenesis when normalized for Y•. As a first step in studying the radical initiation by PCET, R2 was synthesized with Y356 replaced by 3-nitrotyrosine (NO_2Y). The protein is inactive (specific activity 1×10^{-4} that of wt-R2), which permitted a determination of the pK_a of the NO_2Y in the R1/R2 complex in the presence of substrate and effectors. Under all conditions, the pK_a was minimally perturbed. This has important mechanistic implications for the radical initiation process.

Class I ribonucleotide reductases (RNRs)[1] catalyze the conversion of nucleoside diphosphates (NDP) to deoxynucleoside diphosphates (dNDP), supplying all the deoxynucleotides required for DNA replication and repair (*1*). The *Escherichia coli* RNR is composed of two homodimeric subunits: R1 and R2. A 1:1 complex of R1 and R2 is thought to be essential for the reduction process (*2*). R1 binds the NDP substrates and contains the binding sites for the deoxynucleotide triphosphate (dNTP) and adenosine-5′-triphosphate (ATP) effectors that control specificity and rate of RNR turnover (*3*−*6*). R2 harbors a diferric-tyrosyl radical (Y•) cofactor that is essential for initiating nucleotide reduction. Isotope effects, mechanism based inhibitors, site-directed mutants, and electron paramagnetic resonance (EPR) methods have all been used to probe the mechanism of the reduction process (*7*). These studies, in conjunction with the separate crystal structures of R1 (*8*) and R2 (*9*, *10*), have provided us with a reasonably detailed understanding of the chemical mechanism of nucleotide reduction that involves both protein and nucleotide radical intermediates. However, the mechanism of radical initiation is still unresolved: how does the essential Y• in R2 (Y122, *E. coli* numbering used throughout) generate a putative thiyl radical (S•) on C439 in R1, which is proposed to be >35 Å away based on a docking model of the R1 and R2 structures (*8*)? This long distance, and the enzymatic turnover number of 2−10 s^{-1} (*11*), necessitates a

† C.S.Y. and M.C.Y.C. would like to thank the Merck/MIT Collaboration for predoctoral fellowships. Funding was provided by NIH GM29595 (J.S.) and GM47274 (D.G.N.).

* To whom correspondence should be addressed. E-mail: stubbe@mit.edu.

§ Department of Biology.

‡ Department of Chemistry.

[1] Abbreviations: AMP, ampicillin; ATP, adenosine-5′-triphosphate; CDP, cytidine-5′-diphosphate; CBD, chitin binding domain; DIEA, diisopropylethylamine; DMF, *N*,*N*-dimethylformamide; dNDP, deoxynucleoside diphosphates; DPV, differential pulse voltammetry; DTT, dithiothreitol; equiv, equivalents; ESI-MS, electrospray ionization mass spectrometry; Fmoc, 9-fluorenylmethyl carbamate; HATU, *N*-[(dimethylamino)-1H-1,2,3-triazolo[4,5-b]pyridine-1-ylmethylene]-*N*-methylmethanamunium hexafluorophosphate *N*-oxide; HEPES, *N*-2-hydroxyethylpiperazine-*N*′-2-ethanesulfonic acid; $(His)_6$-R2, hexahistidine tagged R2; HOBT, *N*-hydroxybenzotriazole•H_2O.; IPTG, isopropyl-*β*-D-thiogalactopyranoside; MALDI-TOF, matrix assisted laser desorption ionization time-of-flight mass spectrometry; MeCN, acetonitrile; MESNA, 2-mercaptoethanesulfonic acid; NADPH, reduced *β*-nicotinamide adenine dinucleotide phosphate; NDP, nucleoside diphosphates; NO_2Y, 3-nitrotyrosine; OD, optical density; OPfp, pentafluorylphenyl; PMSF, phenylmethylsulfonyl fluoride; RNR, ribonucleotide reductase; R1, large subunit of RNR; R2, small subunit of RNR; S•, thiyl radical; SDM, site-directed mutagenesis; SF, stopped-flow; TFA, trifluoroacetic acid; Tris, tris(hydroxymethyl)aminomethane; TTP, thymidine-5′-triphosphate; wt, wild-type; Y•, tyrosyl radical.

10.1021/bi0352365 CCC: $25.00
Published on Web 11/20/2003

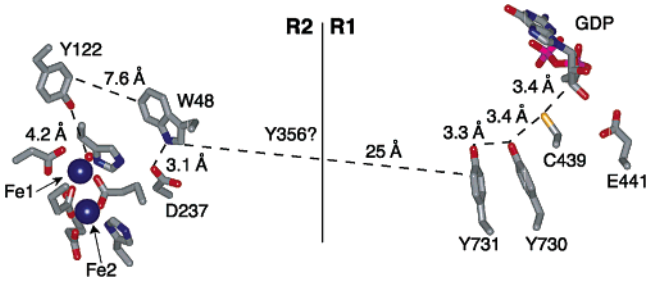

FIGURE 1: Proposed PCET pathway in Class I RNR from *E. coli* based on the docking model of Uhlin and Eklund (*8*). The distance between W48 in R2 and Y731 in R1 is unknown.

pathway for radical transfer involving amino acid radical intermediates (*8*, *12*−*14*). A docking model of R1 and R2 structures, based on shape complementarity and conservation of amino acids in class I RNRs, led to the pathway model shown in Figure 1.

Mutagenesis of the residues in this pathway, and more recent in vivo complementation studies, have demonstrated the importance of these residues (Figure 1) in the nucleotide reduction process (*15*−*19*). Three tyrosines (Y356, Y730, and Y731) are particularly intriguing since they can be transiently oxidized and have no known role in either cofactor assembly (generation of the diferric Y• cluster) or nucleotide reduction. However, neither the long distance of radical initiation nor the involvement of amino acid radical intermediates have been experimentally verified. Only recently have methods been developed to perturb the radical initiation process in a mechanistically informative fashion (*20*, *21*). We now report the semisynthesis of the R2 subunit of RNR using intein technology and solid-phase peptide synthesis that results in 100 mg quantities of protein (*20*, *22*, *23*). We have replaced Y356, one of the putative intermediates on this PCET pathway, with 3-nitrotyrosine (NO_2Y) (Figure 1). The power of the method is demonstrated with the NO_2Y-R2 by measuring the pK_a of a single amino acid within the R1/R2 complex in the presence of substrates and effectors. The observation that the pK_a is not significantly perturbed has important implications in the mechanism of PCET and the gating of this process.

MATERIALS AND METHODS

Materials. All restriction enzymes, Mung bean nuclease, T4 DNA ligase, T4 DNA polymerase, Vent DNA polymerase, calf-intestine alkaline phosphatase used for cloning, chitin resin, and the IMPACT intein purification kit were purchased from New England Biolabs (Beverly, MA). BL21 (DE3) RIL Codon+ competent cells, XL-10 ultracompetent cells, *Pfu* turbo DNA polymerase, and the Quikchange mutagenesis kit were purchased from Stratagene (La Jolla, CA). Plasmid pET-9D was purchased from Novagen (Madison, WI). DNA oligonucleotide syntheses, sequencing, and electrospray ionization mass-spectrometry (ESI-MS) on proteins were performed by MIT Biopolymers Laboratory (Cambridge, MA). Calf-intestine alkaline phosphatase used in the radioactive assays was purchased from Roche (Basel, Switzerland). Miniprep Spin kits, Ni^{2+}-NTA resin, and PCR purification kits used to purify plasmid constructs were from Qiagen (Valencia, CA). Fmoc-Asp(OtBu)-Ser(psiMe,Mepro)-OH, *N*-hydroxybenzotriazole·H_2O (HOBT), and Fmoc-cysteine(*t*Buthio)-pentafluorophenyl ester were purchased from Novabiochem (Weidenmattweg, Switzerland). NO_2Y and Fmoc-NO_2Y were purchased from BAChem (King of Prussia, PA). Fmoc-L-Leu-PEG-PS resin, *N*-[(dimethylamino)-1H-1,2,3-triazolo[4,5-b]pyridine-1-ylmethylene]-*N*-methylmethanamunium hexafluorophosphate *N*-oxide (HATU), disopropylethylamine (DIEA), *N*,*N*-dimethylformamide (DMF), 20% piperidine in DMF, and all other protected amino acids were purchased from Applied Biosystems (Foster City, CA). *N*-L-Acetyltyrosinamide, DNAse I, thymidine-5′-triphosphate (TTP), ATP, cytidine-5′-triphosphate (CDP), reduced β-nicotinamide adenine dinucleotide phosphate (NADPH), trifluoroacetic acid (TFA), 2-mercaptoethanesulfonic acid (MESNA), and Triton X-100 were purchased from Sigma (St. Louis, MO). [^{14}C]-CDP was purchased from Moravek Biochemicals (Brea, CA).

Construction of N-Terminal (His)$_6$-R2 by PCR. PCR was used to generate the desired construct. The N-terminal primer with a hexahistidine tag was 5′-CGA TCG GCC **ATG** GGT CAT CAT CAC CAT CAC CAT ATG GCA TAT ACC ACC TTT TCA CAG ACG-3′. The NcoI restriction site is underlined, and the start codon is in bold. The C-terminal primer was 5′-CTG GTA GGA TCC **TCA** GAG CTG GAA GTT ACT CAA ATC GTC-3′. The BamHI site is underlined, and the stop codon is in bold. The PCR was performed with Vent DNA polymerase. Both the PCR product and pET-9D were doubly digested with 5× excess of NcoI and BamHI and ligated with T4 DNA ligase. The resulting (His)$_6$-R2 contains nine additional residues: methionine, glycine, the hexahistidine tag, followed by the initial methionine of R2.

Site-Directed Mutants of R2. All mutagenesis studies were performed using the QuikChange mutagenesis kit. The primers used are shown in Table 1.

Generation of R2(1−*353)/Intein/Chitin-Binding Domain (CBD) Plasmid Construct.* A plasmid containing an R2(1−353)/intein/CBD construct was generated from pTYB3 (from IMPACT kit). pTYB3 contains a mutated version of the intein coded by *vma 1* of *Saccharomyces cerevisiae* fused to a CBD. pTYB3 contains NcoI and SapI restriction sites in its polylinker region, allowing an inframe fusion of a truncated R2 gene to the intein without the addition of any extra codons. pTYB3 utilizes a T7 promoter that requires isopropyl-β-D-thiogalactopyranoside (IPTG) induction for protein expression; it also includes a gene for ampicillin (AMP) resistance.

pTYB3 was first digested with a 4× excess of SapI for 16 h at 37 °C and purified. The resulting 5′-overhang was filled in using T4 DNA polymerase by incubating the reaction mixture at 12 °C for 20 min. The reaction was stopped by heating at 75 °C for 10 min, and the resulting plasmid was purified.

The DNA was then doubly digested with a 5× excess of NcoI and EcoRI at 37 °C for 1.5 h, and the DNA product was purified. pTYB3 was now linear, with a blunt SapI site and an NcoI sticky end. The plasmid was next treated with calf-intestine alkaline phosphatase (1 U per picomol of DNA blunt ends) for 30 min at 37 °C, and the resulting DNA was purified.

The truncated R2 insert was prepared by PCR from pTB2 (*24*). PCR primers were designed so that the 5′ end of the R2 gene contained an NcoI site that maintains the ATG start codon. The N-terminal primer was 5′-CCA ACA GGA CAC ACC CAT GGC ATA TAC CAC CTT TTC AC-3′. The

Table 1: Primers Used for Mutagenesis Experiments

mutant	antisense primer	sense primer
S354C-R2	5′ GCA GGA AGT GGA AGT CTG TTC TTA TCT GGT CG 3′	5′ CGA CCA GAT AAG AAC AGA CTT CCA CTT CCT GC 3′
S355C-R2	5′ GGA AGT GGA AGT CAG TTG TTA TCT GGT CGG G 3′	5′ CCC GAC CAG ATA ACA ACT GAC TTC CAC TTC C 3′
V353C-$(His)_6$-R2	5′ CCG CAG GAA GTC GAA TGC AGT TCT TAT CTG GTC GGG 3′	5′ CCC GAC CAG ATA AGA ACT GCA TTC CAC TTC CTG CGG 3′
V353A,S354C-$(His)_6$-R2	5′ CCG CAG GAA GTG GAA GCC TGT TCT TAT CTG GTC GGG 3′	5′ CCC GAC CAG ATA AGA ACA GGC TTC CAC TTC CTG CGG 3′
V353G,S354C-$(His)_6$-R2	5′ CGC AGG AAG TGG AAG GCT GTT CTT ATC TGG TCG GG 3′	5′ CCC GAC CAG ATA AGA ACA GCC TTC CAC TTC CTG CG 3′
Y356F-$(His)_6$-R2	5′ GGA AGT CAG TTC TTT TCT GGT CGG GCA GAT TGA 3′	5′ TCA ATC TGC CCG ACC AGA AAA GAA CTG ACT TCC 3′
V353A-R2(1−353)/intein/CDB	5′ GCA GGA AGT GGA AGC CTG CTT TGC CAA GGG 3′	5′ CCC TTG GCA AAG CAG GCT TCC ACT TCC TGC 3′
V353G-R2(1−353)/intein/CDB	5′ CAG GAA GTG GAA GGC TGC TTT GCC AAG GG 3′	5′ GGC AAA GCA GCC TTC CAC TTC CTG CGG 3′

NcoI site is underlined. The C-terminal primer was 5′-ATA ACT CGA GAC TTC CAC TTC CTG CGG AGC-3′. The XhoI site is underlined.

PCR was performed using *Pfu* DNA polymerase, and the product was purified and digested with 5× XhoI for 2 h at 37 °C. The resulting 3′-overhang was removed with Mung bean nuclease (1 U per μg of DNA) for 30 min at 30 °C, then quenched with SDS (0.01%). The DNA fragment was purified, digested with 5× NcoI, and repurified.

The R2 insert was ligated to modified pTYB3 using T4 DNA polymerase and a 5× molar excess of insert over vector. The reaction mixture was incubated at 16 °C for 12 h, and the reaction was stopped by heating at 65 °C for 10 min. The ligation mixture was transformed into XL-10 Ultra-competent cells and plated on LB-AMP plates.

Synthesis of 22mer Peptide by Solid Phase and Solution Phase Chemistry (CSXLVGQIDSEVDTDDLSNFQL). The R2 C-terminal 22mer peptide was synthesized using a combination of standard solid phase and solution phase peptide synthesis methods. The first 19 residues were synthesized using the Pioneer Peptide Synthesizer from Applied Biosystems. The next three amino acids, including NO_2Y at position 20, were coupled manually.

The syntheses employed Fmoc-L-Leu-PEG-PS resin (0.2 mmol of substitution/gram of resin). The amino groups of the amino acids were protected with 9-fluorenylmethyl carbamate (Fmoc). Asparagine and glutamine side chains were trityl protected; serines, tyrosines, aspartates, and glutamates were *t*-butyl protected; the cysteine was protected with a disulfide linked *t*-Buthio group. In place of serine (residue 13) and aspartate (residue 14), the pseudoproline dipeptide, Fmoc-Asp(OtBu)-Ser(psiMe,Mepro)-OH, was used. The phenol hydroxyl of Fmoc-NO_2Y was not protected. HATU was used as the coupling reagent.

Each peptide synthesis cycle began with the removal of the peptidyl N-terminal Fmoc group with 20% piperidine, 0.1 M HOBT in DMF for 10 min (when performing manual reactions, this step was repeated a second time). The coupling reactions utilized 4 equiv of amino acid, 3.6 equiv of HATU, and 8 equiv of DIEA over peptide. Coupling reactions progressed for 1 h. The last amino acid, the protected cysteine, was purchased as a pentafluorylphenyl (OPfp) ester, and coupling was performed with 4 equiv at a final concentration of 0.16 M for 2 h in the absence of HOBT and DIEA.

Peptide Cleavage from the Solid-Phase Resin. Before the peptide was cleaved from the resin, it was washed twice with a small volume of DMF, then twice with a small volume of dichloromethane. All traces of dichloromethane were removed in vacuo. The peptide was then incubated with freshly prepared cleavage mixture (25 mL/gram of resin), consisting of 95% TFA, 2.5% triisopropylsilane, and 2.5% water, for 3−4 h with shaking. All side-chain protecting groups, except for the *t*-Buthio group of the cysteine, were removed in the cleavage step.

The mixture was drained from the reaction vessel, and the resin was rinsed with a small amount of TFA twice. The TFA rinse was combined with the cleavage mixture, and the volume was reduced by the passage of nitrogen over the solution. Peptide precipitation occurred when ∼50% of the TFA was evaporated. Approximately seven volumes of chilled diethyl ether were added, and the mixture was kept at 4 °C to complete the precipitation. The precipitate was then collected by centrifugation, and the supernatant was discarded. The peptide pellet was washed once with cold diethyl ether, and the pellet was redissolved with a minimum volume of 0.1 M NH_4HCO_3, pH 8.0, and lyophilized.

Purification of the 22mer Peptide. Peptide purity was analyzed on a Waters HPLC instrument (Milford, MA) using a C-18 (150 × 4.6 mm, 5 micron) Jupiter column from Phenomenex (Torrance, CA). The peptide was only soluble under basic conditions, which dictated the choice of the purification procedure. Peptide was eluted with a linear gradient from 90% 0.1 M NH_4HCO_3, pH 8.0, 10% acetonitrile (MeCN) to 25% 0.1 M NH_4HCO_3, pH 8.0, 75% MeCN over 45 min at 1 mL/min flow rate. Elution was monitored by UV/vis spectroscopy at 214, 276, and 430 nm. The 22mer peptide typically eluted at 35% MeCN (17 min retention time). Large scale peptide purifications used a Phenomenex C-18 column (300 × 30 mm, 10 micron) Jupiter column, using a flow rate of 10 mL/min. Purified peptide samples were lyophilized and stored at −80 °C.

Peptides were characterized using a Voyager Elite MALDI-TOF MS from Applied Biosystems. The MS was performed under negative mode, using linear detection and α-cyano-4-hydroxycinnamic acid as the peptide matrix.

The concentration of NO_2Y containing peptide was determined spectrophotometrically at pH 8.5 with a Model 8453 spectrometer from Agilent (Palo Alto, CA) using λ_{430} of 4200 M^{-1} cm^{-1} for the 3-nitrotyrosinate (pK_a of 7.2) (*25*).

Deprotection of the 22mer t-Buthio Cysteine. The blocked cysteine peptide was dissolved in 0.1 M NH_4HCO_3 buffer to a concentration of 7 mM. The solution was transferred to a pear-shaped flask, and 0.1 volume of 250 mM tris(hydroxymethyl)aminomethane (Tris), pH 8.0, was added. Solid dithiothreitol (DTT) was added to a final concentration of 20 mM, and the solution was degassed on a Schlenk line. After stirring for 4 h, the reaction was rapidly transferred to a 1000 Da molecular weight cutoff dialysis bag from Spectrum Labs (Rancho Dominguez, CA) and anaerobically dialyzed against 5 mM potassium phosphate buffer, pH 6.0 (2×5 h). After dialysis, the peptide solution was removed from the dialysis bag, frozen, and lyophilized. The peptide was stable at −80 °C for a year.

Growth of R2/Intein/CBD Construct in E. coli. The plasmid containing V353G-R2(1−353)/intein/CBD was transformed into competent BL21 (DE3) RIL Codon+ cells. In a typical growth, a 100 mL of LB culture (100 μg/mL AMP) was inoculated with a single colony, and the cells were grown at 37 °C, with 200 rpm shaking for 12 h. The cells were pelleted by centrifugation and resuspended in 10 mL of LB. This step was repeated, and the suspended cells were used to inoculate large LB cultures (usually 10 L). An inoculation ratio of 100:1 overnight culture to large culture was typical.

The large cultures were grown at 37 °C with shaking at 200 rpm. When A_{600} of 0.75 was attained, the temperature was lowered to 23 °C. Fifteen minutes after the temperature was lowered, IPTG was added to a final concentration of 0.5 mM. After 5−6 h shaking at 23 °C, the cells were harvested yielding ∼2 g of cells per liter. Cells were stored at −80 °C for no longer than two weeks. The desired intein chimera constituted ∼10% of cellular protein.

Purification of V353G-R2(1−353)/Intein/CBD. All purifications were performed at 4 °C. Each gram of V353G-R2(1−353)/intein/CBD containing cells were resuspended in 5 mL of intein buffer (30 mM *N*-2-hydroxyethylpiperazine-*N*′-2-ethanesulfonic acid (HEPES) pH 7.6, 500 mM NaCl, 0.1% Triton X-100) containing 200 μM phenylmethylsulfonyl fluoride (PMSF) and DNAse I (20 μg/g cells). Typically, 50 g of cells were lysed using a French pressure cell at 14 000 psi. $Fe(II)(NH_4)_2(SO_4)_2$ and sodium ascorbate (5 mg of each per gram of cell paste) were dissolved in intein buffer and added dropwise to the lysed cells.

After 15 min of stirring, cell debris was removed by centrifugation for 25 min at 10 000 rpm. The supernatant was loaded onto a chitin resin column preequilibrated with intein buffer. Typically, 10 mL of chitin resin per gram of cell paste was utilized (binding capacity was determined to be ∼2 mg/mL). Column loading flow rates were 1 mL/min. After loading, the column was washed with 30 volumes of intein buffer containing PMSF at 3−4 mL/min. The column was washed with 2 column volumes of cleavage buffer (50 mM HEPES pH 7.6, 500 mM NaCl) at a maximal flow rate. The column was then loaded with 1.5 volumes of cleavage buffer containing 100 mM MESNA (pH was readjusted to 7.6 after the addition of MESNA), and the reaction was carried out for 24−30 h.

The cleaved protein was eluted with four column volumes of 50 mM HEPES pH 7.6 and 500 mM NaCl and concentrated to 200 μM R2 using a YM-30 membrane (Millipore). Concentration and dilution was repeated 2× to reduce the MESNA concentration. Holo protein purifications had a reddish tint after the cleavage step. This red color, which may be associated with an iron complex, was removed by the concentration and dilution steps.

The concentrated protein (∼200 μM) was gently degassed on a Schlenk line and placed in a 4 °C refrigerator in a glovebox. Lyophilized, deprotected 22mer peptide was also brought into the glovebox and dissolved in degassed water to a concentration of 7 mM. The ligation mixture contained ∼100 μM cleaved R2 and 2 mM peptide and was stirred in the refrigerator in the glovebox for 30−36 h. SDS−PAGE gel (12%) was used to determine ligation efficiencies.

Ligation products consisted of three dimeric forms of R2: full-length homodimers, heterodimers, and truncated homodimers. Purifications were performed with a Mono-Q HR16/10 anion-exchange column from Amersham Biosciences (Piscataway, NJ) using a Biocad Sprint instrument (Applied Biosystems). Before loading, R2 was typically treated with 5 mM DTT and incubated at 4 °C for 30 min to reduce any intermolecular disulfide bonds. Approximately 10 mg of protein can be successfully separated per run. The protein was purified using the following elution gradient at a flow rate of 3 mL/min: 50 mM Tris, pH 7.6, 1.5 mM DTT, 5% glycerol isocratically for 2 min, followed by a linear gradient from 0 to 200 mM NaCl in 2−5 min, from 200 to 440 mM NaCl to 42 min, and from 440 to 700 mM NaCl to 45 min. Full-length R2 eluted at ∼360 mM NaCl. Full-length homodimeric protein was concentrated using a YM-30 Centriprep concentrator (Millipore; Bedford, MA) and frozen at −80 °C.

Growth and Purification of $(His)_6$-R2. A plasmid containing a $(His)_6$-R2 was transformed into competent BL-21 (DE3), and the bacteria were plated on LB-kanamycin plates. A 100 mL culture grown in LB (40 μg/mL kanamycin) was inoculated with a single colony and shaken at 200 rpm overnight at 37 °C for 12 h. The culture was centrifuged and resuspended in 10 mL of LB. This step was repeated, and the suspended cells were used to inoculate large LB cultures. An inoculation ratio of 100:1 (overnight culture/large culture) was typical.

The large cultures were shaken at 37 °C until A_{600} 0.7 was reached. 1,10-Phenanthroline was added to these cultures at a final concentration of 100 μM (prepared as a 100 mM stock solution in 0.1 M HCl) (*26*). The cells were inoculated with 0.5 mM IPTG 15 min after the addition of 1,10-phenanthroline. The cultures were shaken for an additional 4 h, harvested by centrifugation, and stored at −80 °C. $(His)_6$-R2 constituted ∼45% of the cellular protein.

For purification, each gram of cell paste was resuspended in 5 mL of $(His)_6$-R2 buffer (50 mM Tris, 500 mM NaCl, 10 mM imidazole, 200 μM PMSF, pH 7.6), and DNAse I (20 μg/g cell paste) was added to the resuspended cells. The cells were lysed by passage through a French pressure cell at 14 000 psi, and the cell debris was cleared by centrifugation for 25 min at 10 000 rpm. The supernatant was loaded onto Ni^{2+}-NTA resin (3 mL of resin per gram of cell paste). The column was then washed with 20 column volumes of $(His)_6$-R2 buffer. The bound protein was eluted with $(His)_6$-R2 buffer containing 250 mM imidazole (the buffer pH was readjusted after the addition of imidazole). The eluted protein was dialyzed against R2 buffer (50 mM Tris, 5% glycerol, pH 7.6) overnight with one change of buffer. To remove heterodimers of wt-R2 and $(His)_6$-R2, the dialyzed protein

was further purified using a Ni^{2+}-affinity MC/M 10 × 100 column from Applied Biosystems. The gradient employed was from 50 mM Tris, pH 7.6, 5% glycerol to 50 mM Tris, pH 7.6, 5% glycerol and 125 mM imidazole over 15 min at 1 mL/min flow rate. The protein eluted at 7 min. After chromatography, the protein was concentrated to 8 mg/mL and stored at −80 °C.

Assembly of (His)$_6$-R2 Di-Iron-Y•. Apo(His)$_6$-R2 was gently degassed on a Schlenk line and brought into the glovebox, opened to the atmosphere, and placed in the refrigerator at 4 °C. Fe(II)$(NH_4)_2(SO_4)_2$ was dissolved in degassed water in the glovebox, and the concentration of Fe(II) was determined with the Ferrozine assay (*27*). Fe(II) (5 equiv per equivalent of apo(His)$_6$-R2) was added to the protein. After 15 min, the protein was removed from the glovebox, and 3.5 equiv of O_2 was added at 4 °C. The Y• content was determined spectrophotometrically (*28*) and was typically 1.2−1.3 radicals/dimer.

ESI-MS of R2 Constructs. Purified R2 constructs were characterized by ESI-MS. Typically, 20 μL of R2 (>75 μM) was exchanged into water using Micro Bio-Spin 30 columns from Bio-Rad (Hercules, CA). The samples were diluted to a final concentration of ∼5 μM with 50% MeCN, 50% water, and 0.2% acetic acid immediately before analysis. Approximately 1−5 pmol of the diluted samples was loaded onto a PE Sciex API365 Triple Quad instrument from Applied Biosystems via direct infusion at 5 μL/min, and data were collected under positive mode.

Radioactive Assays using Y356F-(His)$_6$-R2 and NO_2Y-R2. A typical assay mixture contained in a final volume of 380 μL: 1.0 mM [^{14}C]-CDP (4720 CPM/nmol), 3.0 mM ATP, 3 mM NADPH, 30 μM TR, 0.5 μM TRR, and 3 μM R1 and R2 in 50 mM HEPES, pH 7.6, 15 mM $MgSO_4$, 1 mM EDTA. The ratio of R1 to R2 was 1:1. Reactions at 25 °C were initiated by the addition of R1. At time zero, a 50 μL aliquot of the reaction mixture was removed before the addition of R1. Aliquots (50 μL) were then removed over 30 min and quenched with 25 μL of 2% perchloric acid or heating in a boiling water bath. Acid-quenched samples were neutralized with 19 μL of 0.5 M KOH. After all the time points were collected, 10 U of calf-intestinal alkaline phosphatase (Roche) and 400 nmol of dC in 100 mM Tris, pH 8.5, 0.5 mM EDTA were added to a final volume of 1.0 mL and incubated at 37 °C for 2 h. Aliquots (950 μL) were loaded onto 1.7 mL Dowex-1 borate columns, and dC was isolated by the procedure of Steeper and Steuart (*29*). The columns were washed with 8 mL of water. Eluent (1.0 mL) was added to 9.0 mL Emulsifier−Safe scintillation fluid (Packard Biosciences) and analyzed for radioactivity using a Beckman LS-6500 scintillation counter (Fullerton, CA). One unit of RNR activity is defined as 1 nmol of dCDP produced/min.

Determination of the pK_a of NO_2Y in NO_2Y-R2. 3-Nitrophenolate has an λ_{428} of 4200 $M^{-1}cm^{-1}$ *(25)*. To determine the pK_a of NO_2Y in R2, absorption spectra from 350 to 650 nm as a function of pH were determined with a Cary-3 spectrophotometer (Varian; Walnut Creek, CA). The pH of each solution was measured using a micro pH electrode from Orion (Beverly, MA). Samples at pH 6.75 and below were buffered with 50 mM MES, samples between pH 7.0 and 8.0 were buffered with 50 mM HEPES, samples at pH 8.25 and above were buffered with 50 mM TAPS. All samples contained 15 mM $MgSO_4$ and 1 mM EDTA. Six sets of experiments were carried out: the first used the 22mer peptide at 20 μM; the second contained R2 at 10 μM; the third contained R1 and R2 at 10 μM; the fourth contained R1 and R2 at 10 μM and TTP (100 μM); the fifth contained R1 and R2 at 10 μM, ADP (1 mM), and dGTP (100 μM); the sixth contained R1 and R2 at 10 μM, CDP (1 mM), and TTP (100 μM). To compensate for differences in baseline absorptions, all spectra were zeroed at 650 nm.

Preparation of the N-Acetyl-3-nitrotyrosinamide. NO_2Y (800 mg, 3.5 mmol) was dissolved in 17 mL of methanol, 5.2 mL (71.3 mmol) of thionyl chloride was added dropwise with stirring, and the reaction allowed to proceed for 2 days. At this time, the excess thionyl chloride was removed in vacuo and triturated several times with CH_3OH. The NO_2Y methyl ester was obtained in >95% yield.

The ester (2 mmol) was dissolved in 20 mL of MeCN with 4 equiv of triethylamine and 1.5 equiv of acetic anhydride, and the reaction mixture was stirred for 2 h. The solvent was then removed in vacuo resulting in a mixture (85:15) of the *N*-acetylated derivative and the di-N,O-acetylated derivative. The mixture of compounds (1 mmol) was used without further purification by dissolving them in 20 mL of methanol saturated with ammonia. The reaction was monitored by silica gel thin-layer chromatography (TLC) in 6:1 chloroform/methanol (R_f of starting material and product were 0.8 and 0.5, respectively). The reaction was >95% complete by 50 h at which time the solvent was removed in vacuo. The product was purified in >90% yield by silica gel chromatography (5 × 25 cm), using 9:1 chloroform/methanol as eluent.

^{1}H NMR (d_6-DMSO): δ 7.98 (d, J = 7.5 Hz, 1 H), 7.60 (d, J = 3 Hz, 1 H), 7.45 (s, 1 H), 7.20 (m, 2 H), 6.48 (d, J = 8.0 Hz, 1 H), 4.28 (ddd, J = 6, 8, 8 Hz, 1 H), 2.75 (dd, J = 6, 14 Hz, 1 H), 2.5 (dd, J = 8, 14 Hz, 1H), 1.75 (s, 3 H).

Electrochemical Measurements. Differential pulse voltammetry (DPV) measurements were performed on *N*-acetyl-3-nitrotyrosinamide and *N*-acetyltyrosinamide, using a CV-50W instrument from Bioanalytical Systems (West Lafayette, IN) as previously described (*30*). Measurements were performed with a three-electrode glass cell, with a glassy carbon working electrode, a platinum wire counter-electrode, and a Ag/AgCl/3M NaCl reference electrode. The glassy carbon electrode was polished with a water/alumina slurry and sonicated before each measurement.

Sample solutions contained a 200 μM tyrosine analogue and 200 μM potassium ferricyanide in 3 mL of 10 mM potassium phosphate, 200 mM KCl adjusted to the appropriate pH with HCl or KOH. Potassium ferrocyanide has a redox potential of 436 mV at pH 7.0 and served as an internal standard. Each measurement was performed with a different sample. All solutions were degassed by N_2 sparging for several minutes prior to measurement. The data were fit to the following equation: $E_p = E_p(Y^•/Y^-) + 2.303RT/nF \log(1 + 10^{-pH}/10^{-pK_{red}})$. $E_p(Y^•/Y^-)$ is the peak potential of the oxidation of $Y^- \rightarrow Y^•$, and pK_{red} is the pK_a of $Y \rightarrow Y^- + H^+$.

RESULTS

Previous studies to examine the feasibility of a pathway involving amino acid radical intermediates in the radical

Scheme 1: Semisynthesis of R2 Using Intein Mediated Ligation

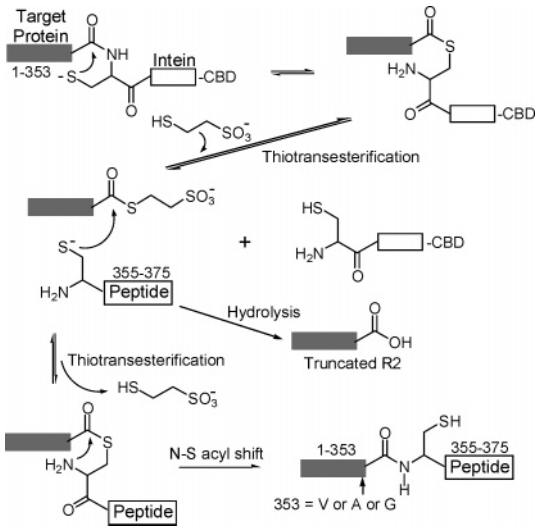

initiation process of class I RNRs have utilized site-directed mutagenesis to replace amino acids proposed to be on the pathway. Unfortunately, this method is limited to natural amino acids. Substitution of Y with F (Figure 1), for example, dramatically perturbs the residue's reduction potential and also disrupts the proposed coupling of proton and electron transfers. The ability of a residue's protonation state to modulate its reduction potential is thought to be an essential component of the radical initiation process by proton-coupled electron transfer (PCET) (*12*, *30*). To overcome these limitations, we have synthesized R2 semisynthetically. This technique allows us to substitute Y356 of R2 with any unnatural amino acid by ligating the thioester of R2(1−353), prepared by intein technology, to the peptide 354−375, synthesized by solid-phase peptide methods. The overall strategy for this semisynthetic approach is shown in Scheme 1, and the rationale for the choices made at various stages of this synthesis are presented.

Synthesis of Peptide 354−375 (CSXLVGQIDSEVDTDDLSNFQL) (X Is Y or NO_2Y). One essential step in preparing semisynthetic R2 was the synthesis of the R2 C-terminal peptide, the 22mer-CSXLVGQIDSEVDTDDLSNFQL. The peptide containing residues 1−19 was made using solid-phase methods, and residues 20−22 were added manually. Solid-phase peptide synthesis was carried out using standard Fmoc protected amino acids, polystyrene beads with a poly(ethylene glycol) linker, and HATU as the coupling agent (*31*). Problems involving aspartimide formation, low amino acid coupling efficiencies after attachment of residue seven due to the peptide's unusual secondary structure, and the peptide's acid insolubility had to be overcome to generate the required amounts of peptide for R2 synthesis at a reasonable cost.

During reverse-phase HPLC purification of the 19mer peptide, a variable amount of a second product was encountered. This side product had a longer retention time and a mass of 67 Da larger than the desired product. After extensive detective work, we established that the increased mass was associated with intramolecular aspartamide formation (probably associated with D14), followed by ring opening with the piperidine used in the removal of the Fmoc blocking group. Formation of this side reaction was subsequently minimized by the addition of HOBT (0.1 M) to the Fmoc deblocking solution (*32*), and the reduction in the concentration of piperidine in this solution from 25 to 20%. While 20% piperidine is the standard concentration used in Fmoc deprotections, we had employed 25% in an effort to improve deprotection efficiencies.

The secondary structure of the peptide limited access to its amino terminus, resulting in both poorer Fmoc deprotection and amino acid coupling efficiencies. This problem became progressively worse as the peptide chain length increased. Coupling of L19 to sterically hindered V18 proved especially difficult. Use of a pseudoproline dipeptide (Asp(O*t*-Bu)-Ser(ψMe,Mepro)-OH) in place of S13 and D14 in the synthesis introduced a kink in the peptide's amide backbone, which disrupted secondary structure and alleviated all of these problems (*33*). During the TFA cleavage step, protecting groups of the pseudoproline dipeptide are removed, yielding a free aspartate and serine. The pseudoproline dipeptide also prevented aspartamide formation at position D14.

Amino acid residues, 20−22, were added manually so that Fmoc protected tyrosine analogues such as Fmoc-NO_2Y could be added in parallel at position 20. The N-terminal C354 was coupled using a cysteine derivative whose carboxylate was activated with a OPfp group and whose side chain was protected as the *t*-Bu disulfide group. The OPfp group allowed coupling in the absence of DIEA (*34*), thereby limiting cysteine racemization, while the *t*-Bu disulfide protecting group allowed peptide purification under basic conditions.

Purification under basic conditions was required because the crude 22mer peptide was insoluble in acid. The preponderance of acidic groups in the sequence is incompatible with typical TFA purification protocols using C-8 reverse-phase HPLC methods. NH_4HCO_3 (0.1 M) buffers were thus used for peptide purification (Figure 2A). The peptides purified by this procedure where judged to be >95% homogeneous, and MALDI-TOF mass spectrometry using α-cyano-4-hydroxycinanamic acid as a matrix gave molecular masses identical within error to those calculated (Figure 2B).

Identification of the Best Site for Ligation. In addition to peptide synthesis, thioester activated truncated R2 must be generated for ligation and full-length R2 production (Scheme 1). As a first step in determining the best site for peptide ligation, a number of R2 site-directed mutants were prepared. A major concern was that the placement of a cysteine near Y356 could result in uncoupling of the normal electron transfer (ET) pathway and inactivation of RNR by $Y^{\bullet}$ loss. S354C-R2 and S355C-R2 constructs were generated by site-directed mutagenesis, and the mutant R2s were purified and assayed for activity. The results, shown in Table 2, suggest that based on activity, S354 is a better choice than S355 for the ligation site. However, both mutants exhibited a slow, time-dependent inactivation, in contrast with wt-R2, when nucleotide reduction was monitored over a 30 min period. The rate of inactivation increased with increasing pH (Figure 3). RNR activity could not be determined at pH >9.1 due to protein precipitation. The pH dependence of the inactivation process suggests uncoupling by ET through oxidation of the thiolate at C354 or C355 (data not shown) since the reduction potential for cysteine is decreased 0.6 V upon

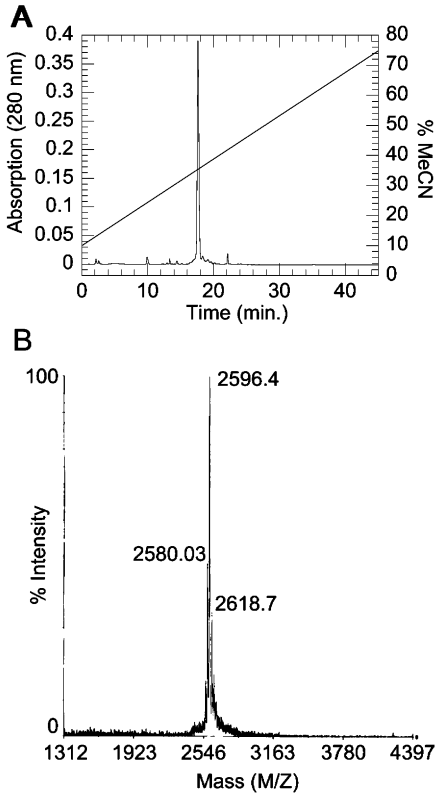

FIGURE 2: (A) Reverse-phase HPLC profile of the crude 22mer peptide with NO_2Y at position X. (B) MALDI-TOF spectrum of the purified NO_2Y-22mer peptide. Calculated mass: 2595 Da; observed mass: 2596 Da.

Table 2: Specific Activity of Different R2 Constructs Determined by the Spectrophotometric Assay

protein	specific activity (nmol min^{-1} mg^{-1})	radicals/dimer
wt-R2	6000	1.2
S354C-R2	4500	1.0
S355C-R2	2000	1.2
$(His)_6$-R2	6000	1.2
V353C-$(His)_6$-R2	1650	0.9
V353G,S354C-$(His)_6$-R2	1500	1.2
V353A,S354C-$(His)_6$-R2	3500	0.85

deprotonation (*35*). Indeed, the loss of $Y^{\bullet}$ during the course of the assay was observed using the spectrophotometric dropline correction method (*28*) (data not shown). Despite the slow inactivation, a large number of turnovers prior to inactivation, even at elevated pHs, is observed. At pH 7.0, after 10 min, 550 dCDPs are generated and at pH 9.0, after 10 min, 120 dCDPs are produced (data not shown). These observations suggested that S354 is a reasonable choice for the ligation site.

In addition to the site of ligation, we also considered the size of the amino acid preceding the ligation site. Previous studies suggested that ligation sites containing bulky amino acids often reduce the ligation efficiency (*36*). Sequence comparisons of R2s further revealed that residue 353 is not conserved and can be occupied by a glycine, leucine, isoleucine, glutamine, or serine. We thus generated V353A, S354C, and V353G, S354C double mutants by site-directed mutagenesis, and their activities and $Y^{\bullet}$ content were determined (Table 2). The S354C-R2 had a specific activity of 4500 nmol min^{-1} mg^{-1}, while the V353A and V353G double

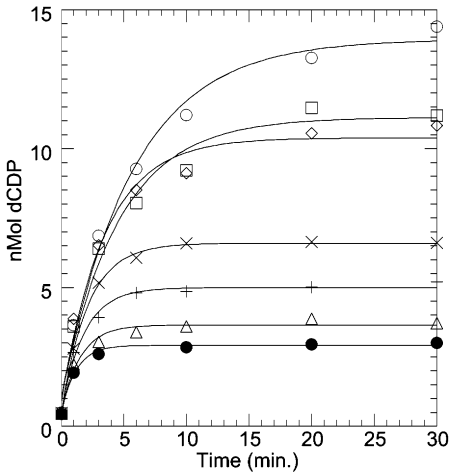

FIGURE 3: Activity assays (*29*) of V353G,S354C-$(His)_6$-R2 prepared by site-directed mutagenesis at various pHs: (○) pH 7.6; (□) pH 8.0; (◇) pH 8.25; (×) pH 8.5; (+) pH 8.75; (△) pH 9.0; and (●) pH 9.1. A typical assay contained 1.5 μM R1, 0.5 μM R2, 3.0 mM ATP, and 1.0 mM CDP.

mutants had specific activities of 3500 and 1500 nmol min^{-1} mg^{-},[1] respectively. From these studies, we chose to locate the new peptide bond between residues 353 and 354, with a glycine at 353. Despite the reduced activity of this mutant (25% of wt-R2s), the less bulky glycine greatly enhanced the ligation efficiency and provided the protein quantities required to study PCET.

Generation of R2 (1−353)-Intein-CBD. As illustrated in Figure 1, Y356 is in the putative radical initiation pathway. In all the R2 crystal structures, the C-terminal 30−40 amino acids are not detectable due to thermal lability. In the *E. coli* R2 structure (*37*), only residues 1−340 are visible (*9*). Thus, we fully expected that the C-terminus of R2 (1−353) would be accessible for ligation without requiring protein denaturation. The commercially available yeast intein *vma1* was used to make the desired intein construct (*22*). The DNA was manipulated as described in the Materials and Methods, and the resulting protein, after assembly of the di-iron $Y^{\bullet}$ cofactor (*24*), was readily purified with a chitin affinity column. A similar construct was also generated with a $(His)_6$-C-terminal tag replacing the CBD. Use of the $(His)_6$-C-terminal tag was abandoned in favor of the CBD tag since the chitin affinity column allowed larger amounts of more homogeneous R2 to be isolated.

Problems Encountered during Cleavage of R2(1−353) from the Intein/CBD Domain and Ligation with the Peptide. Several major technical problems during cleavage/ligation were encountered that require further comment. If the cell paste containing this construct was stored at −80 °C for more than two weeks, amide product due to the S to N acyl shift between residue 353 of R2 and the intein and loss of the reactive thioester were observed (Scheme 1). The generation of the desired thioester construct was therefore carried out within several days of bacterial growth.

A second problem was the timing of the generation of the diferric $Y^{\bullet}$ cofactor essential for R2 activity (*28*). Cluster assembly was attempted at several stages during the construction of the semisynthetic R2. The best protein recoveries were obtained when the diferric $Y^{\bullet}$ cluster was assembled before isolation of the truncated R2/intein/CBD construct. In our hands, truncated R2 and full-length R2 in their apo

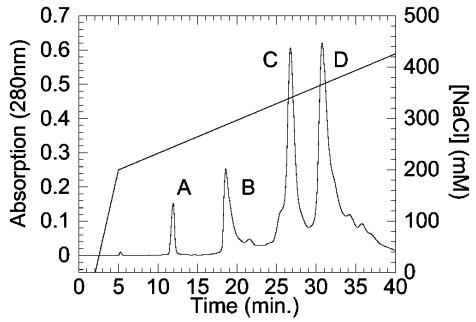

FIGURE 4: Purification of NO_2Y-R2 by Mono-Q HR16/10 chromatography. Peak A, peptide; peak B, truncated homodimer; peak C, truncated/full-length heterodimer; and peak D, full-length homodimer.

forms are much less stable than cofactor assembled R2. Thus, the earlier the cluster is inserted, the higher the overall recoveries of the full-length product.

A third technical problem involved the choice of the intein thioester cleavage reagent (Scheme 1). The ideal reagent should cleave the R2/intein thioester with high efficiency, yet also be a good leaving group, thus promoting efficient ligation of the synthetic peptide to the cleaved R2. The reagent needs to be sufficiently reactive in each of these steps to compete with thioester hydrolysis. We examined MESNA, thiophenol, β-mercaptoethanol, ethanethiol, and DTT as cleavage agents. Generally, DTT effected cleavage with the highest efficiencies, but the yields of the subsequent ligation step with the synthetic peptide were poor (<25%). Ligation efficiencies of the DTT truncated R2s improved only marginally with the addition of catalytic amounts of thiophenol (*38*) or MESNA. Overall, cleavage with MESNA proved optimal, maintaining adequate cleavage efficiency and the highest ligation efficiencies.

In addition to the choice of reagent, the identity of the amino acid at the cleavage site (353), as noted previously, proved to be crucial. When 353 is valine (as in wt-R2), cleavage efficiencies with all thiol reagents investigated were low (less than 5%). Cleavage efficiencies where V353 was replaced with the less bulky alanine were equally poor when using MESNA as the cleavage reagent. Cleavage efficiency of the alanine mutant with DTT was approximately 45%, but as noted previously, the ligation efficiencies with DTT were low, causing us to abandon this construct. Replacing V353 with a glycine resulted in the highest cleavage efficiencies (approximately 50% when using MESNA as the cleavage reagent). Ligation efficiencies with the MESNA cleaved glycine mutant were also high and generally between 60 and 80%. We thus chose the MESNA cleaved V353G construct for all subsequent studies since it provided the best combination of cleavage yield and ligation efficiency.

Ligation of the 22mer Peptide with R2 (1−353) Thioester and R2 Purification. The R2 (1−353) MESNA analogue eluted from the chitin binding column was concentrated to ~100 μM and incubated with the desired peptide (2 mM) for 30−36 h in the glovebox at 4 °C. The long ligation time required for this bimolecular reaction resulted in some hydrolysis of the thioester R2 construct (Scheme 1).

Semisynthetic R2 was purified from the truncated homo and heterodimeric R2s by anion-exchange chromatography. This separation was successfully achieved because of the negatively charged C-terminal tail of R2 (Figure 4). The

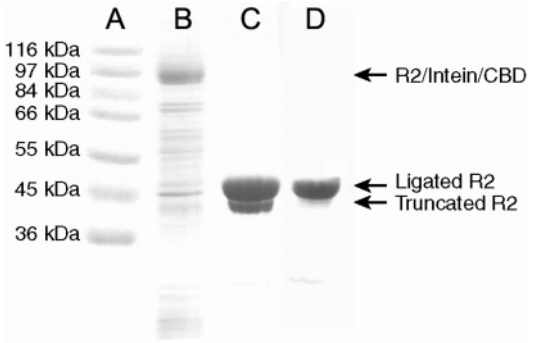

FIGURE 5: Purification of NO_2Y-R2 monitored by SDS−PAGE. (A) Molecular weight markers; (B) crude cell lysate showing expression of V353G-R2(1−353)/intein/CBD at 91.7 kDa; (C) ligation mixture showing 80:20 mixture of full-length ligated R2 to truncated R2; and (D) full-length NO_2Y-R2 isolated from Mono-Q column (Figure 4).

Table 3: Molecular Weight of Different R2 Constructs Determined by ESI-MS

protein	expected mass (Da)	observed mass (Da)
wt-R2	43 386	43 394, 43 568
C268S-R2	43 370	43 378, 43 553
apo V353G,S354C-$(His)_6$-R2	44 371	44 377, 44 554
holo V353G,S354C-$(His)_6$-R2	44 371	44 550, 44 726
apo C305S,V353C-$(His)_6$-R2	44 385	44 390, 44 567
NO_2Y-R2	43 406	43 402, 43 580
V353G,S354C-R2 prepared semi-synthetically	43 360	43 364, 43 540

purity of the material is routinely established by SDS−PAGE (Figure 5) and by ESI-MS. Typically, 1.5 mg of the purified, full-length, ligated R2 could be obtained from 1 g of cell paste. The final semisynthetic R2s contained 0.7−1.2 $Y^{\bullet}$ per dimer. A control experiment revealed that the specific activities of G353,S354-R2 prepared by the intein method and by site-directed mutagenesis were identical when normalized for tyrosyl radical content.

ESI-MS Characterization of R2 Constructs. Direct infusion ESI-MS analyses of the many R2 constructs, prepared semisynthetically and by site-directed mutagenesis, revealed the expected masses within the error of the method. However, a second species with a mass 170−180 Da greater than the expected mass of the R2 construct was also observed in all cases in variable amounts (Table 3). This species was present in wt-R2, $(His)_6$-R2 mutants, as well as the semisynthetic R2. Although we have thus far been unable to identify the nature of the chemical modification, we do know that the activity of the wt-R2 does not appear to be affected by it.

Peak Potential for Blocked NO_2Y using Differential Pulsed Voltammetry. The choice of NO_2Y as one of our first replacements for Y356 was based on our supposition that this analogue might prevent dCDP formation due to the increased difficulty in oxidizing NO_2Y relative to tyrosine. We used the method described by Tommos et al. (*30*) to compare the reduction potentials of the acylated and amide protected forms of tyrosine and NO_2Y. The results of these experiments are shown in Figure 6, with a blow-up of the pH range from 6.5 to 9.0 (Figure 6B) in which RNR can be assayed. At pH 7.0, the measured peak potential for blocked tyrosine is 1.02 V, which compares well with 1.04 V, previously reported (*39*). At pH 6.5, the blocked NO_2Y is

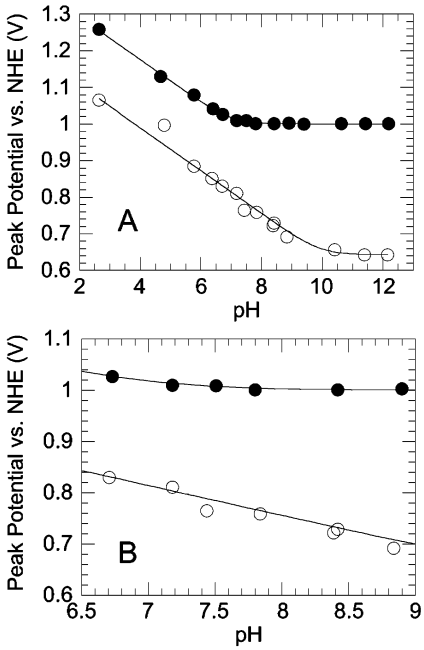

FIGURE 6: Differential pulse voltammetry from pH 2.5 to 12.5 of *N*-acetyltyrosinamide (○) and *N*-acetyl-3-nitrotyrosinamide (●). (A) Data over the entire pH range. (B) Data over the pH range in which R2 can be assayed. Instrument settings: sensitivity, 100 μA/V; scan rate, 10 mV s^{-1}; sample width, 17 ms; pulse amplitude, 50 mV; pulse, 50 ms; pulse period, 200 ms; and quiet time, 4s (*30*).

more difficult to oxidize than blocked Y by 200 mV, while at pH 9.0 the difference increases to 300 mV. It is of interest to determine if this change in driving force completely blocks nucleotide reduction.

Activity of Y356X-R2s. R2 is an essential gene, and expression of R2 mutants and determination of their activities in *E. coli* is complicated by the contaminating wt-R2 that typically forms heterodimers with mutant R2s. A lower limit of detection for deoxynucleotide formation has thus been between 1 and 8% of wt activity, depending on the overexpression levels of a particular mutant. Therefore, to establish a lower limit of detection for a mutation in residue 356, we have used an affinity-based purification that allows a separation of mutant R2 from the wt-R2. Y356F-R2 with a $(His)_6$ at its N-terminus was generated and induced in the presence of 1,10-phenanthroline to minimize iron incorporation (*26*). The apo Y356F-$(His)_6$-R2 was purified with Ni^{2+}-NTA gravity-flow columns, and then the diferric-Y• cluster was assembled. This protein had an activity 3.5×10^{-4} that of wt-R2. Further purification of this mutant with a MC/M Ni^{2+} affinity column using a Biocad Sprint FPLC system allowed removal of additional heterodimer, giving mutant R2 with activity $<5 \times 10^{-5}$ that of the wt. At present, this is our lower limit of detection and serves as the standard by which R2 mutants with unnatural amino acids in position 356 are judged. A control with wt-R2 containing the same N-terminal tag gave the identical Y• content and specific activity as the untagged wt-R2.

The results of an activity assay on the NO_2Y-R2, monitoring the rate of dCDP formation using [^{14}C]-CDP, in comparison with $(His)_6$-R2 Y356F are shown in Figure 7. The actual activity of this mutant was difficult to measure as the enzyme appears to undergo inactivation with time, as was observed with V353G, S354C-$(His)_6$-R2 (Figure 3). The

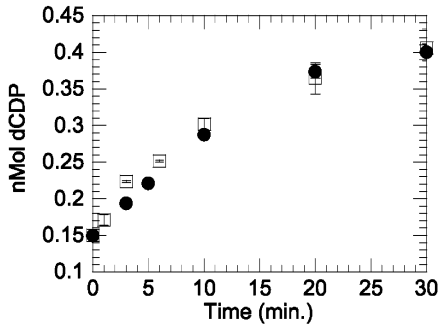

FIGURE 7: Activity assay of NO_2Y-R2 (□) and Y356F-$(His)_6$-R2 (●) with equimolar amounts of R1 at pH 7.6. The concentration of NO_2Y-R2 was 3.0 μM and Y356F-$(His)_6$-R2 was 1.5 μM, and CDP had a specific activity of 4720 CPM/nmol.

results reveal that the activity is approximately 1×10^{-4} that of the wt-R2. The activity of Y356F-$(His)_6$-R2 (purified by use of only the first Ni^{2+} column) is approximately 2× higher and also exhibits a slow time-dependent inactivation similar to dCDP formation using NO_2Y-R2. Given the small amounts of dCDP formed with NO_2Y-R2 (1−2 equiv per equivalent of R2), it is difficult to determine whether the NO_2Y-R2's activity is due to NO_2Y-R2's inherent activity or small amounts of contaminating wt-R2 heterodimers. A distinction between these two possibilities is important mechanistically but at present cannot be made.

pK_a of a NO_2Y of R2 within the R1/R2 Complex. Models for long-range radical initiation involving PCET dictate the importance of the pK_as of the aromatic amino acids and cysteine in tuning their redox potentials and potentially in minimizing charge separation by hydrogen atom transfer (*40*). In addition, the proton on the phenol of tyrosine might play an important role in conformational triggering of the PCET in the presence of substrate and allosteric effector. How the protein environment modulates the pK_a of a residue such as Y356 and its reduction potential are essential to our understanding of the radical initiation and is presently unknown. Several experiments were therefore designed to measure the pK_a of NO_2Y-R2 when complexed with R1; with R1 and effector TTP; with R1, CDP, and TTP; and with R1, ADP, and dGTP. These pK_as can be compared with the pK_a of this residue in the R2 alone and in the 22mer peptide.

The results of these experiments are shown in Figure 8 and the apparent pK_as reported in Table 4. The pK_a of NO_2Y in the peptide is 7.1, identical to that observed in R2 alone. When R2 is complexed with R1, R1, and TTP and the active form R1, ADP, and dGTP, the pK_as shift to 7.2, 7.3, and 7.4, respectively. In a second active complex with R1, CDP, and TTP, the pK_a is shifted to approximately 8.0. The instability of this complex precluded obtaining any data at pH >9.0 and therefore a good endpoint. The shift in pK_a supports complex formation between R1 and R2. This shift, however, is small relative to the perturbations observed in a number of catalytic systems (*41*, *42*). The total change in A_{430} observed in all of the titration experiments is similar to that predicted from the concentration of the R2 and the extinction coefficient of a blocked NO_2Y. The λ_{max} at 430 nm of the phenolate appears not to be shifted by the protein environment (see difference spectrum, Figure 9). Thus, the long wavelength of the nitrophenolate and the ability to titrate its proton within the physiological pH range has provided a

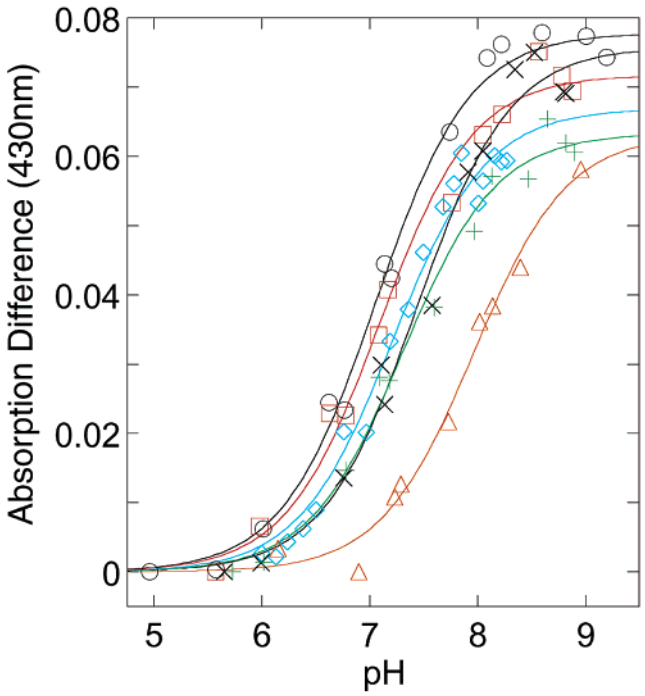

FIGURE 8: Titration of NO_2Y monitoring the conversion of the phenol to the phenolate at 430 nm. Black (○) 20 μM NO_2Y-peptide; red (□) 10 μM NO_2Y-R2; cyan (◊) 10 μM R1 and NO_2Y-R2; black (×) 10 μM R1 and NO_2Y-R2 and 0.1 mM TTP; green (+) 10 μM R1 and NO_2Y-R2, 0.1 mM dGTP, and 1.0 mM ADP; brown (△) 10 μM R1 and NO_2Y-R2, 0.1 mM TTP, and 1.0 mM CDP. The data were fit to the following equation: $A = \epsilon_H K_a[H^+] + (\epsilon^-[NO_2Y])/(K_a[H^+] + 1)$ (*47*). A is absorption at 430 nm; ϵ_H and ϵ_- are the extinction coefficients of protonated and deprotonated NO_2Y at 430 nm, respectively; K_a is the dissociation constant; and $[NO_2Y]$ is the total concentration of protonated and deprotonated NO_2Y.

Table 4: pK_a Values of NO_2Y Determined from pH Titrations

sample	pK_a
22mer peptide	7.1
R2	7.1
R1/R2[a]	7.2
R1/R2/TTP	7.4
R1/R2/ADP/dGTP	7.3
R1/R2/CDP/TTP[a]	8.0

[a] Enzyme instability in these R1/R2 complexes at pHs greater than 9 precluded an accurate determination of titration endpoints.

unique opportunity to monitor pH dependent changes of the R1/R2 complex. If the pH dependence of the NO_2Y is indicative of the behavior of other tyrosines in this position, then their pK_as are minimally perturbed due to the R1/R2 interface environment, even in the presence of substrates and effectors.

DISCUSSION

The problem of radical initiation in the class I RNRs appears to be unique. Most ET reactions in biology proceed very rapidly and irreversibly over 10−15 Å (*14*, *43*). In the case of RNR however, the Y122• on R2 is proposed to generate a transient S• on R1, upon binding of substrate and effector to R1. Additionally, the stability of the Y122• and the reversibility of the PCET on each turnover (*11*) have made this a challenging problem to investigate. The putative long range (35 Å) for radical initiation in class I RNRs is based on a docking model proposed by Uhlin and Eklund

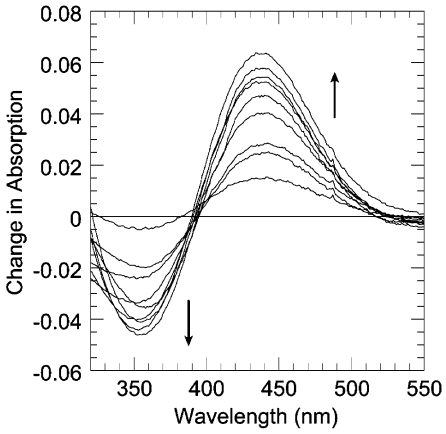

FIGURE 9: NO_2Y-R2/R1/TTP/CDP titration difference spectra. The absorption spectrum of the sample obtained at pH 5.75 was subtracted from all other spectra. Arrows indicate decrease of phenol (A_{360}) and increase of phenolate (A_{430}) as pH increases.

(*8*) from the independent structures of R1 and R2 and their shape complementarity. Using the Marcus−Levich equation, one can calculate the rate constant for ET, when the driving force and reorganization energies are optimized, to be between 10^{-6} to 10^{-9} s^{-1} over such a distance if one assumes β values between 1.2 and 1.4 $Å^{-1}$ (*44*). Since the turnover number of RNRs varies from 2 to 10 s^{-1}, depending on the substrate and effector, the radical initiation cannot occur over this long distance without intermediates. The only intermediates possible are aromatic amino acid radicals (Figure 1). Thus, if no large conformational reorganization of R1 and R2 occurs during complex formation, then this system would represent the first physiologically relevant example of the participation of amino acid radical intermediates in transporting a redox hole over long distances (>8 Å). Efforts to detect intermediates in hole migration in this system using site-directed mutants of members of the putative pathway have been unsuccessful (*15*−*19*). In fact, detection of transient intermediates in long-range hole migration in any system, including DNA (shown to proceed over 200 Å), has thus far been unsuccessful (*12*). In the case of RNR, the interesting but negative results from the mutagenesis studies demonstrate that alternative technologies are essential to understand the radical initiation process.

Clearly, it is important to establish the validity of the docking model, specifically the distances between Y122• in R2 and the C439 in R1. Recently, we have used pulsed electron−electron double resonance spectroscopic methods to measure the distance between the two Y•, one in each monomer of R2 (*45*). Using mechanism based inhibitors that label the active site of R1, we are confident that we can generate a construct in which the key distance between the Y• of R2 and the active site of R1 can be measured.

In this paper, we have shown that R2 can be made semisynthetically with a NO_2Y uniquely at position 356. After many technical setbacks presented in the Results, isolation of these mutant R2s made semisynthetically in 100 mg quantities is now possible. Large amounts of material are required for SF−UV/vis and rapid freeze quench EPR methods to test the pathway model for radical initiation and for detection of intermediates. Some issues in R2 construction, such as identification of the molecule(s) that modify R2s by 170 Da, remain to be resolved. However, the high

specific activities of the R2s constructed by the intein method in comparison with the wt-R2s and R2s prepared by site-directed mutagenesis give us confidence that our semisynthetic constructs can be instrumental in unraveling the mechanism of the radical initiation process.

We have recently reported the first results using R2 made semisynthetically in which Y356 was replaced by 2,3-difluorotyrosine (F_2Y) (*20*). This construct was used to test the model that communication between W48 on R2 and C439 on R1 involves a series of hydrogen atom transfer reactions (*15*, *17*, *18*, *40*, *46*). The pK_a of *N*-acetyl C-esterified F_2Y is 7.8 in aqueous solution, and its redox potential is very similar to that of tyrosine's. Our proposal was that examination of the pH rate profile for nucleotide reduction using this mutant R2 could test the hydrogen atom transfer model directly. Under conditions in which the analogue is protonated, deoxynucleotide should be generated with a rate similar to wt-R2, and when F_2Y is deprotonated, no deoxynucleotide should be generated. The results of the study showed that deoxynucleotide was generated from pH 6.0 to 9.0, with a pH profile very similar to that observed with the wt-R2 made by the intein procedure. If the pK_a of the F_2Y is not significantly perturbed in the R1/R2 complex, then the direct coupling of proton and electron transfer for migration between W48 and Y731 is no longer a requirement for radical initiation. In the case of the F_2Y, this pK_a is difficult to measure as its absorption features are very similar to tyrosine's. We therefore turned to NO_2Y-R2, which offers a unique spectroscopic handle for measuring a single pK_a within a protein of 260 000 Da molecular weight. Titrations of R1/R2, R1/R2 in the presence of effector, and R1/R2 in the presence of substrate and effector indicate that the pK_a is minimally perturbed relative to free peptide and free R2 (Figure 8). Assuming one can extrapolate from our observation of minimal pK_a perturbation with the NO_2Y-R2 to the case of F_2Y-R2, then one can conclude that the hydrogen atom transfer model between W48 of R2 and Y731 of R1 is not essential. This result is perhaps not surprising as the docking model (Figure 1) demands that the distance between Y356 and its adjacent partners on the pathway (probably ~12 Å) is too far to involve direct hydrogen atom transfer without large conformational changes. Whether the redox potential of Y356 or its derivatives is perturbed by the protein environment still remains an open issue. The similarity in the pH profile of wt and F_2Y-R2, however, suggests that it is not greatly perturbed, as the conformational change gating ET still appears to be rate limiting (*11*).

In the case of the NO_2-Y356-R2, we hypothesized that its reduction potential would be perturbed sufficiently relative to tyrosine's to prohibit its oxidation by the putative W48$^{\bullet}$ or W48H$^{+\bullet}$ in the ET pathway. The reduction potential of *N*-acetyl-tyrosinamide relative to *N*-acetyl-3-NO_2-tyrosinamide (Figure 6) is perturbed 200 mV at pH 6.5 and 300 mV at pH 9.0. This perturbation can be contrasted with the 40−110 mV perturbation of F_2Y-R2 at the same pH extremes. Thus, it was of interest to determine if this reduction potential perturbation would be sufficient to change the rate limiting step from a conformational change (*11*) to PCET or serve as a complete thermodynamic block to ET. Activity studies with Y356F-$(His)_6$-Y2, in which the phenylalanine is not oxidizable within the physiological pH range, have allowed us to set a lower limit of detection for deoxynucleotide formation of 5×10^{-5} that of wt-R2. Deoxynucleotide formation, greater than 1 equiv per equivalent of NO_2Y-R2, was detected at a rate of 1×10^{-4} that of wt-R2. DeoxyNDP formation was not linear with time, an observation that we initially associated with loss of the Y$^{\bullet}$ on R2 via uncoupling through a thiolate at C354. However, when the Y356F-R2 (with a serine at 354) was examined for dNDP formation over the same time period, the rate also appeared to drop off with time. Thus, at present we cannot distinguish between a very small amount of activity associated with NO_2Y-R2 and activity associated with a small amount of heterodimer with wt-R2. Tyrosine analogues with reduction potentials intermediate between F_2Y-R2 and NO_2Y-R2 are required to establish if the rate determining step has actually been altered and to elucidate the importance of tyrosine's pK_a in tuning the reversible PCET.

Summary. The intein technology to generate R2 now offers a unique tool to investigate the radical initiation process in the class I RNRs. The availability of a wide range of tyrosine derivatives with altered redox potentials and pK_as suggests that this approach will be informative with respect to the determination of the validity of the PCET model. In addition, this technology can be used to place photoaffinity labels and spin labels in the R2 C-terminal tail to test the docking model for complex formation between R1 and R2.

REFERENCES

1. Jordan, A., and Reichard, P. (1998) *Annu. Rev. Biochem. 67*, 71−98.
2. Thelander, L. (1973) *J. Biol. Chem. 248*, 4591−4601.
3. Brown, N. C., and Reichard, P. (1969) *J. Mol. Biol. 46*, 39−55.
4. Thelander, L., and Reichard, P. (1979) *Annu. Rev. Biochem. 48*, 133−158.
5. Kashlan, O. B., and Cooperman, B. S. (2003) *Biochemistry 42*, 1696−1706.
6. Kashlan, O. B., Scott, C. P., Lear, J. D., and Cooperman, B. S. (2002) *Biochemistry 41*, 462−474.
7. Licht, S., and Stubbe, J. (1999) *Mechanistic Investigations of Ribonucleotide Reductases* (Barton, S. D., Nakanishi, K., Meth-Cohn, O., and Poulter, C. D., Ed.) pp 163−203, Elsevier Science, New York.
8. Uhlin, U., and Eklund, H. (1994) *Nature 370*, 533−539.
9. Nordlund, P., Sjoberg, B. M., and Eklund, H. (1990) *Nature 345*, 593−598.
10. Nordlund, P., and Eklund, H. (1993) *J. Mol. Biol. 232*, 123−164.
11. Ge, J., Yu, G., Ator, A. A., and Stubbe, J. (2003) *Biochemistry 42*, 10071−10083.
12. Stubbe, J., Nocera, D. G., Yee, C. S., and Chang, M. C. (2003) *Chem. Rev. 103*, 2167−2201.
13. Gray, H. B., and Winkler, J. R. (2001) *Electron transfer in metalloproteins* (Balzani, V., Ed.) pp 3−23, Wiley-VCH, Weinheim, Germany.
14. Page, C. C., Moser, C. C., Chen, X., and Dutton, P. L. (1999) *Nature 402*, 47−52.
15. Ekberg, M., Sahlin, M., Eriksson, M., and Sjoberg, B. M. (1996) *J. Biol. Chem. 271*, 20655−20659.
16. Ekberg, M., Potsch, S., Sandin, E., Thunnissen, M., Nordlund, P., Sahlin, M., and Sjoberg, B. M. (1998) *J. Biol. Chem. 273*, 21003−21008.
17. Rova, U., Goodtzova, K., Ingemarson, R., Behravan, G., Graslund, A., and Thelander, L. (1995) *Biochemistry 34*, 4267−4275.
18. Rova, U., Adrait, A., Potsch, S., Graslund, A., and Thelander, L. (1999) *J. Biol. Chem. 274*, 23746−23751.
19. Ekberg, M., Birgander, P., and Sjöberg, B.-M. (2003) *J. Bacteriol. 185*, 1167−1173.
20. Yee, C. S., Chang, M. C. Y., Ge, J., Nocera, D. G., and Stubbe, J. (2003) *J. Am. Chem. Soc. 125*, 10506−10507.
21. Wang, L., and Schultz, P. G. (2002) *Chem. Commun. 1*, 1−11.
22. Xu, M. Q., and Evans, T. C., Jr. (2001) *Methods Enzymol. 24*, 257−277.

23. Ayers, B., Blaschke, U., Camerero, J., Cotton, G. J., Holford, M., and Muir, T. W. (1999) *Biopolymers 51*, 343−354.
24. Salowe, S. P., and Stubbe, J. (1986) *J. Bacteriol. 165*, 363−366.
25. Tawfik, D., Chap, R., Eshhar, Z., and Green, B. (1994) *Protein Sci. 7*, 431−434.
26. Baldwin, J., Krebs, C., Ley, B. A., Edmondson, D. E., Huynh, B. H., and Bollinger, J. M., Jr. (2000) *J. Am. Chem. Soc. 122*, 12195−12206.
27. Stookey, L. L. (1970) *Anal. Chem. 42*, 779−782.
28. Bollinger, J. M., Jr., Tong, W. H., Ravi, N., Huynh, B. H., Edmondson, D. E., and Stubbe, J. A. (1995) *Methods Enzymol. 258*, 278−303.
29. Steeper, J. R., and Steuart, C. D. (1970) *Anal. Biochem. 34*, 123−130.
30. Tommos, C., Skalicky, J. J., Pilloud, D. L., Wand, A. J., and Dutton, P. L. (1999) *Biochemistry 38*, 9495−9507.
31. Bodanszky (1993) *Peptide Chemistry: A Practical Textbook*, Springer-Verlag, Berlin, Germany.
32. Lauer, J. L., Fields, C. G., and Fields, G. B. (1995) *Lett. Pept. Sci. 1*, 197−205.
33. Mutter, M., Nefzi, A., Sato, T., Sun, X., Wahl, F., and Wohr, T. (1995) *Pept. Res. 8*, 145−153.
34. Han, Y. X., Albericio, F., and Barany, G. (1997) *J. Org. Chem. 62*, 4307−4312.
35. Stubbe, J., and van der Donk, W. A. (1998) *Chem. Rev. 98*, 705−762.
36. Dawson, P. E., Muir, T. W., Clarklewis, I., and Kent, S. B. H. (1994) *Science 266*, 776−779.
37. Eklund, H., Uhlin, U., Farnegardh, M., Logan, D. T., and Nordlund, P. (2001) *Prog. Biophys. Mol. Biol. 77*, 177−268.
38. Dawson, P. E., Churchill, M. J., Ghadiri, M. R., and Kent, S. B. H. (1997) *J. Am. Chem. Soc. 119*, 4325−4329.
39. DeFilippis, M. R., Murthy, C. P., Broitman, F., Weinraub, D., Faraggi, M., and Klapper, M. H. (1991) *J. Phys. Chem. 95*, 3416−3419.
40. Siegbahn, P. E., Erikkson, L., Himo, F., and Pavlov, M. (1998) *J. Phys. Chem. B 102*, 10622−10629.
41. Highbarger, L. A., Gerlt, J. A., and Kenyon, G. L. (1996) *Biochemistry 35*, 41−46.
42. Nabedryk, E., Breton, J., Hienerwadel, R., Fogel, C., Maentele, W., Paddock, M. L., and Okamura, M. Y. (1995) *Biochemistry 34*, 14722−14732.
43. Gray, H. B., and Winkler, J. R. (1996) *Annu. Rev. Biochem. 65*, 537−561.
44. Williams, R. J. P. (1997) *J. Biol. Inorg. Chem. 2*, 373−377.
45. Bennati, M., Weber, A., Antonic, J., Perlstein, D. L., Roblee, J., and Stubbe, J. (2003) *J. Am. Chem. Soc.*, in press.
46. Siegbahn, P. E. M., Blomberg, M. R. A., and Pavlov, M. (1998) *Chem. Phys. Lett. 292*, 421−430.
47. Itoh, S., Takayama, S., Arakawa, R., Furuta, A., Kimatsu, M., Ishida, A., Takamuku, S., and Fukuzumi, S. (1997) *Inorg. Chem. 36*, 1407−1416.

BI0352365